PCCP

Accepted Manuscript

ROYAL SOCIETY OF CHEMISTRY

www.rsc.org/pccp

Renewable fuel by photohydrogenation of CO_2: Impact of the nature of Cu species loaded TiO_2

Bo-Ren Chen [1], Van-Huy Nguyen [1], Jeffrey C.S. Wu [1,*], Reli Martin [2], Kamila Kočí [2]

[1] Department of Chemical Engineering, National Taiwan University, Taipei 10617, Taiwan

[2] Institute of Environmental Technology, VŠB-Technical University of Ostrava, 17. listopadu 15/2172, Ostrava –Poruba 708 33, Czech Republic.

* Corresponding author

Phone: +886-2-23631994, Fax: +886-2-23623040, E-mail: cswu@ntu.edu.tw

9 **Graphical abstract**

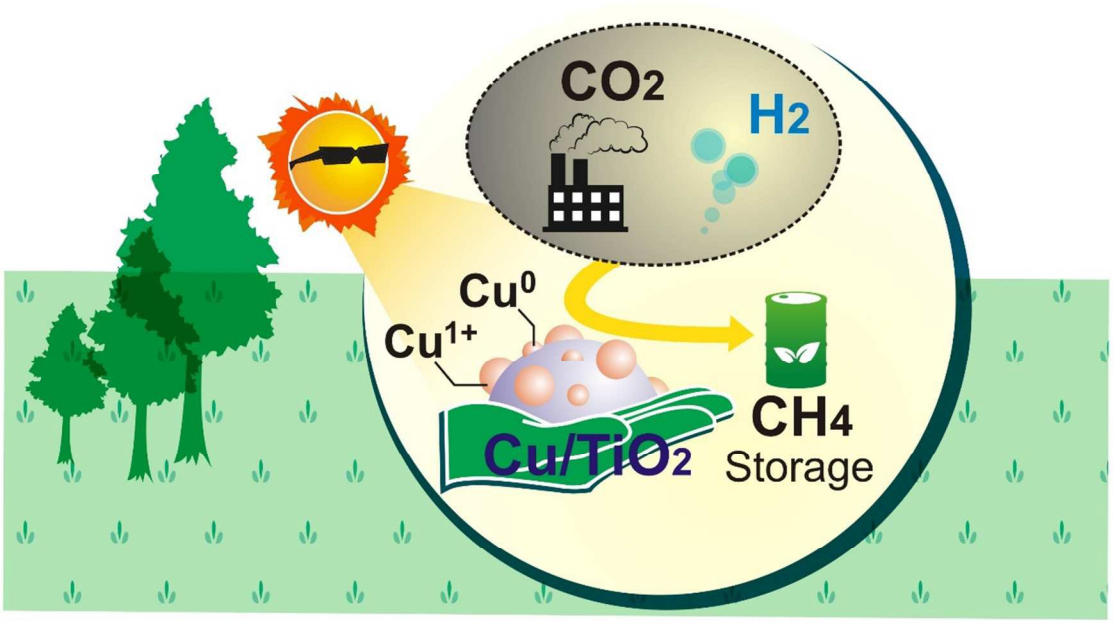

10

11 Efficient gas-phase photocatalytic hydrogenation of CO_2 opens a feasible route not only to store

12 H_2 by converting into renewable fuel but also to cut down the atmospheric CO_2 greenhouse gas.

Abstract

Efficient gas-phase photocatalytic hydrogenation of CO_2 into desired fuel is achieved on Cu-loaded TiO_2 photocatalyst system. Firstly, the enhancing amount of Ti^{3+} rather than Ti^{4+} species in Cu-loaded TiO_2, in comparing with TiO_2 photocatalyst, provides an excellent opportunity to promote the photohydrogenation of CO_2. Additionally, the coexistence of Cu and Cu^{1+} species during the photoreaction could also efficiently enhanced photocatalytic activity by prolonging the lifetime of electrons. To achieve the best photo-activity, the content of Cu species must be maintained at an appropriate low concentration (≤ 1wt.%), and the corresponding highest CH_4 yield was 28.72 μmol g^{-1}. This approach opens a feasible route not only to store hydrogen converting into desired renewable fuel but also to cut down the atmospheric CO_2 greenhouse gas.

Keywords: photohydrogenation, carbon dioxide; renewable fuel, photocatalysis; Cu-loaded TiO_2

1. Introduction

Nowadays, hydrogen (H_2) is considered as energy for the future because of its clean energy, most abundant, flexible and highly efficient. Although the outlook will inevitably belong to H_2, there are still growing concerns about the H_2 storage.[1, 2] In details, it requires 11,250 l to achieve 1 kg of H_2 under atmospheric pressure and room temperature. Even H_2 is compressed at 700 bars; its volumetric energy density is approximately six times lower than that of gasoline (8.8 kWh/l). Meanwhile, the volumetric energy density of natural gas, which mainly consists of methane (CH_4), has four- to fivefold higher than that of hydrogen.[3] Hence, great efforts have been made to increase the volumetric energy of hydrogen.[4] On the other hand, we also concern how to reduce the atmospheric carbon dioxide (CO_2), which is the major greenhouse gas in Earth's atmosphere.[5, 6]

To solve these issues, H_2 storage through hydrogenation of CO_2 to hydrocarbons has been successfully developed.[7, 8] Ideally, this concept provides an alternative and sustainable pathway for H_2 storage by considering greenhouse gas CO_2 as a potential building block.[9] It allows H_2 to be converted into renewable fuel, which directly resolves both global environment and H_2 storage issues. Among many alternative processes, photohydrogenation of CO_2, which is an ideal method for converting CO_2 into desired fuels, is considered with much attention.[10-12] However, it is noted that the quantum efficiency and product yield in the CO_2 photohydrogenation are still low and requires a further study. The design of photocatalyst which works efficiently for the photohydrogenation of CO_2 has been the subject of several studies. Among the candidates, titania-supported copper catalyst plays a crucial role in promoting the photocatalytic reduction of CO_2.[13-16] Additionally, supported copper is found to be economical and abundant in nature.

Herein, a series of Cu/CuO loaded TiO_2 was synthesized and carried out the photohydrogenation of CO_2 with H_2O in the single photoreactor. It is noticeable that the oxidation state of Cu species is a crucial factor in CO_2 photoreduction activity.[15] Hence, the impact of reducing CuO to Cu and the transition of Cu species during the reaction were carefully evaluated for their potential to hydrogenation. Furthermore, chemical and structural features of photocatalysts were thoroughly characterized by SEM, XRD, UV-vis, XPS and XANES.

2. Experimental

2.1. Preparation of photocatalysts

The whole synthesis procedure is shown in Scheme 1. Titanium dioxide (denoted as TiO_2) photocatalyst was prepared by a sol-gel method, which was adapted from Tseng et al.[15] A typical batch contained 21 ml titanium (IV) butoxide ($Ti(OC_4H_9)_4$, 99 %, Fluka), 22 ml *n*-butanol (C_4H_9OH, 99.4 %, J.T. Baker) and 14 ml acetic acid (CH_3COOH, 99.7 %, J.T. Baker). The mixed solution was stirred for 8 h. Then, the transparent sol was dried at room temperature to 423 K for 3 h in an oven, then transferred to a furnace and calcined at 773 K for 5 h to burn off hydrocarbons and consequently produce the desired TiO_2 powder photocatalyst.

Titania-supported copper oxide (denoted as CuO/TiO_2) photocatalyst was prepared by an impregnation method. TiO_2 powder, which was previously prepared, was added to an appropriate amount of copper (II) chloride solution ($CuCl_2$, 99 %, Sigma-Aldrich). The solution was then sonicated in an ultrasonic bath and mixed with a magnetic stirrer to get a homogeneous slurry. After wet impregnation, it was dried at 353 K and finally calcined in air at 773 K for 4 h. For titania-supported copper metal (denoted as Cu/TiO_2) photocatalyst, it was prepared by reducing

of CuO/TiO_2 under a flow of 5% H_2/N_2 mixture at 573 K for 3 h. In our research, we named each photocatalyst with different Cu/CuO loading weight percentage.

2.2. Characterization of photocatalysts

The light absorption of photocatalysts was fully characterized by UV-visible spectrophotometer (UV-vis, Varian Cary-100). $BaSO_4$ was used as the absorption standard in these measurements. Powder X-ray diffractometer (XRD, Bruker-D8-ADVANCE) with a Cu Kα (λ = 1.5418Å) radiation source at 40 kV and 40 mA was used to verify the crystalline structure of the photocatalysts. The BET specific surface area of photocatalyst was determined by N_2 adsorption using Physisorption Analyzer (Micromeritics ASAP 2000). Field emission scanning electron microscopy (FE-SEM, JEOL JSM-7000) integrated with energy dispersive spectroscopy (EDS) was operated at an acceleration voltage of 5 kV. The photocatalysts were sputtered with a thin layer of Pt film to prevent surface charging. The X-ray photoelectron spectroscopy (XPS, Thermo Scientific Theta Probe) was used to determine the oxidation states of the elements. The X-ray absorption near-edge structure (XANES) at the Cu K-edge was recorded at the BL17C1 beamline, National Synchrotron Radiation Research Center (NSRRC), Taiwan, where the electron storage ring was operated at an acceleration voltage of 1.5 GeV. All data were acquired at an ambient temperature in the fluorescence mode. The K-edge data was normalized to equal the edge jump.

2.3. Photocatalytic hydrogenation of CO_2

The gas-phase photocatalytic hydrogenation of CO_2 with H_2O was carried out in a single Pyrex photoreactor with the volume of 385 ml (as shown in Figure 1). Photocatalyst powder (0.10 g) was evenly packed on the Teflon flat that was fixed in the middle of photoreactor. The bottom of photoreactor was moisturized with 5 ml of deionized water to tune the saturated water vapor pressure in the photoreactor through controlling the reaction temperature. The pen-ray lamp (11SC-1, 254 nm, 12 mW cm^{-2}) was put from the top of photoreactor to irradiate the UV-light. Before the photoreactions, the reactor was first purged with the CO_2 for 30 min, and tightly closed at an ambient pressure. Then, H_2 (0.01 atm) was added to the photoreactor. After that, the photoreactor was heated up to 363 K by heating tape to generate the gaseous H_2O, and the lamp was switched on to start the experiment.

The reaction products collected in the gas phase were analyzed every 2 h during the irradiation by gas chromatography (China GC-FID 9800) integrated with the flame ionization detector. To analyze the CO, a methanizer packed with Ni catalyst was connected to GC-FID to convert CO into CH_4 with H_2 at 633 K. A Porapak Q column was installed, and pure N_2 was used as the carrier gas for FID in the detection of hydrocarbons.

The photoreduction quantum efficiency (PQE) is calculated as follows:

$$\text{PQE (\%)} = 100\% \times (n \times \text{product formation rate}) / \text{incident photon rate} \quad (1)$$

Here, n is the number of moles of photoelectrons required to generate one mole of reduction product from CO_2, which includes CH_4 and CO. The incident photon rate is determined from the incident light intensity at $\lambda = 254$ nm and projected light irradiation area.

The blank experiments were also conducted before performing the photocatalytic reaction. There were almost no products or below the detection limit of gas chromatography with any part

112 missing, including (a) photocatalysts and (b) UV-light source. Evidently, the photocatalytic
113 hydrogenation of CO_2 is mainly photo-catalyzed.

114

115 **3. Results and discussion**

116 **3.1. Photocatalyst characterization**

117 All photocatalysts were fully characterized by BET, FE-SEM, EDS, UV-vis, XRD, XPS and
118 XANES to reveal their structure, surface morphology and chemical state of the species. Firstly,
119 the morphology of the synthesized TiO_2 and Cu-loaded TiO_2 is examined by FE-SEM, as shown
120 in Figure 2. It clearly indicates that loading of Cu obviously could not change the shape and
121 modify the morphology of supported TiO_2. However, the dispersion of Cu species might
122 decrease with increasing loading amount. The mapping photograph for 2%CuO/TiO_2
123 photocatalyst and their corresponding elemental mapping of Ti, O and Cu was shown in Figure 3.
124 It clearly shows that a part of the Cu-loaded could be aggregated. It is not beneficial for the
125 photocatalytic activity. By the elemental EDS analysis, the weight percentages of Cu species in
126 1%Cu/TiO_2 and 2%Cu/TiO_2 are 0.95 and 2.31 wt%, respectively, which is consistent with the
127 composition as planned.

128 Figure 4 depicts the XRD patterns of the TiO_2 along with Cu-loaded TiO_2 photocatalysts. All the
129 photocatalysts exhibited similar XRD patterns. A very sharp and intense peak was observed at 2θ
130 = 25.28° corresponds to the (101) planes of the anatase TiO_2, while few small peaks were also
131 observed at 2θ values of 36.95°, 37.80°, 38.58°, 48.05°, 53.89°, 55.06°, 62.69°, 68.76°, 70.31°,
132 75.03°, and 76.02°, respectively. These values are in good agreement with anatase phase (JCPDS,
133 No. 21-1272), suggesting that crystallite structure of TiO_2 exists mostly as anatase phase. The

inset of Figure 4 shows the shift of the (101) planes of the anatase TiO_2 peaks toward lower 2θ values in the patterns of Cu-loaded TiO_2, suggesting that Ti sites in the TiO_2 lattice were occupied by Cu species.[17] Although we have observed the (101) planes of the anatase TiO_2 peaks changed significantly in intensity, only a slight change in half width was observed. The TiO_2 crystallite sizes were estimated from the half bandwidth of the corresponding X-ray spectral peak by the Scherrer formula:

$$D = k\lambda/(\beta \cos\theta) \quad (2)$$

Here, λ is the X-ray wavelength (λ = 1.5418Å), β is the half width of the (101) planes, θ is the Bragg diffraction angle, and k is a correction factor (k = 0.9).

In this study, the TiO_2 crystallite sizes were about 31.4-34.0 nm (Table 1), which is consistent with SEM result. It is noted that there are no apparent peaks for CuO in the XRD patterns of CuO/TiO_2. The reason is that the amount of Cu species is very low, in the range of 1-2 wt%; hence, it could not be ruled out due to limitations of the experimental technique. For Cu/TiO_2, the peak at 2θ values of 43.3° and 50.4°, corresponding to Miller indices (111) and (200) planes of metallic Cu species, respectively.[18]

The optical properties of the TiO_2 together with Cu-loaded TiO_2 photocatalysts are measured by UV-vis spectra. As displayed in Figure 5, it clearly shows that all the photocatalysts performed the absorption peak of 360 nm, assigned to TiO_2. The Cu-loaded TiO_2 photocatalysts have an extended absorption edge in the region of 400-800 nm. Interestingly, the UV-Vis spectroscopic studies could gain information on the state of Cu species in these catalysts.[19] As expected, the upward shift of intensity absorbance in this region increased with the loading amount of Cu species. It is noticeable that the broadband of CuO/TiO_2 photocatalysts in the range of 600-800

nm corresponds to d–d transitions of Cu^{2+} in Oh symmetry with a tetragonal distortion.[17] This observation implies that Cu^{2+} species was mainly presented on CuO/TiO_2 photocatalysts. Additionally, pretreatment the photocatalyst by H_2 to reduce the CuO to Cu will raise the band located at 410-590 nm, which corresponds to metallic Cu^0 species.[19, 20] It is noted that this range is also associated with the three-dimensional Cu^{1+} clusters in the CuO matrix due to incomplete reduction.[19]

The oxidation state of Cu species is a key factor that determines their photocatalytic activity in the photoreduction of CO_2.[15] X-ray photoelectron spectroscopy (XPS) was conducted to determine further the chemical environment of Cu species. XPS spectra of the Cu2p region for TiO_2, $2\%Cu/TiO_2$, and $2\%CuO/TiO_2$ photocatalysts are reported (Figure 6(a)). There is no peak observed in the range of 925-965 eV for TiO_2 photocatalyst. In contrast, the $Cu2p_{3/2}$ and $Cu2p_{1/2}$ binding energy values of $2\%CuO/TiO_2$ photocatalyst appeared at 933.9 eV and 953.6 eV, respectively, confirming the presence of Cu^{2+}. It is noted that pretreatment the $2\%CuO/TiO_2$ photocatalyst by H_2 to successfully reduce the Cu^{2+} to Cu^0. The $Cu2p_{3/2}$ and $Cu2p_{1/2}$ binding energy values of $2\%Cu/TiO_2$ photocatalyst appeared at 931.6 eV and 951.8 eV, respectively. These results are in accordance with an earlier report.[21] Due to the low amount of Cu species on $1\%CuO/TiO_2$ and $1\%Cu/TiO_2$ samples, its XPS spectra of the Cu2p region could not be observed clearly. Figure 6(b) shows the Ti2p region for TiO_2, $2\%Cu/TiO_2$, and $2\%CuO/TiO_2$ photocatalysts. The binding energy values appeared at 458.7 eV and 457.3 eV corresponded to Ti^{4+} and Ti^{3+}, respectively.[22] There is a significant amount of Ti^{3+} rather than Ti^{4+} observed in the Ti2p XPS spectra of $2\%Cu/TiO_2$, and $2\%CuO/TiO_2$, in compared with TiO_2 photocatalysts. On the other hand, we also observed a shift to higher binding energy for O1s spectra when Cu species was introduced to the TiO_2 (Figure 6(c)). The O1s binding energy of TiO_2 was at 529.9

eV while those of Cu-loaded/TiO_2 was at 530.6 eV. The loading Cu could modify the surface hydroxyl (O_H) content of photocatalyst.[23]

To have a clearer image of the Cu state on 1%Cu/TiO_2 and 1%CuO/TiO_2 photocatalysts, Cu K-edge XANES was characterized. Figure 7(a) shows the Cu K-edge XANES spectra of 1%Cu/TiO_2 and 1%CuO/TiO_2 photocatalysts, in compared with the Cu foil, Cu_2O and CuO references. The good resemblance spectra of 1%Cu/TiO_2 and 1%CuO/TiO_2 with that of Cu foil and CuO references indicates that their local structure in 1%Cu/TiO_2 and 1%CuO/TiO_2 photocatalysts are mainly in Cu^0 and Cu^{2+}, respectively. There are four types of peaks in a range of 8960-9040 eV, including 1s-3d transition (A), 1s-4p_z (1s-4pπ*) transition (B), 1s-4$p_{x,y}$ (1s-4pσ*) transition (C), and multiple scattering (D).[24] The spectrum of 1%CuO/TiO_2 exhibits a well-separated weak pre-edge band A due to the 1s-3d transition and an intense band B and C due to the 1s-4p transition. However, the band B, which could be observed as a shoulder of the intense band C, is not clearly separated. Additionally, with the presence of a band D (multiple scattering), it suggests that the Cu species on 1%CuO/TiO_2 are aggregated.[24] For the 1%Cu/TiO_2 spectrum, there are no peaks attributed to the band A and D. More importantly here, the Fourier transforms (FTs) of the $k^3\chi(k)$ EXAFS for 1%Cu/TiO_2 and 1%CuO/TiO_2 photocatalysts along with Cu foil, Cu_2O, and CuO references were also compared in Figure 7(b). Phase shift function was used as reference files to analyze the EXAFS data. In the 1%Cu/TiO_2 photocatalyst, the FT peak appearing at 2.45 Å is assigned to Cu-Cu bond. In the 1%CuO/TiO_2 photocatalyst, the first FT peak appearing at 1.84 Å is assigned to Cu-O bond. However, different from the above XANES result, the FT for 1%CuO/TiO_2 photocatalyst in the range of 2-4 Å is not similar to that for the CuO reference but is somewhat similar to that for the Cu_2O reference. In particular, it exhibits only one peak appearing at 3.00 Å, which is assigned to Cu-Cu bond.

In summary, Cu species were successfully loaded on TiO_2 using the incipient wetness impregnation method. Based on the UV-vis, XRD, XPS, and XANES results, the Cu^{2+} mainly exists on CuO/TiO_2 photocatalyst. Importantly, most Cu species in the photocatalysts was stable in Cu^0 after reduction by H_2. The presence of Cu species exhibits outstanding the optical properties. It expects that Cu-loaded TiO_2 can significantly influence the photoreduction of CO_2.

3. Photocatalytic hydrogenation of CO_2

3.1 The presence of hydrogen and reaction temperature

Figure 8 shows the time profiles of the photocatalytic reduction of CO_2 with H_2O in the presence/absence of H_2 under different temperature on $1\%Cu/TiO_2$ photocatalyst. Firstly, we conducted the photoreduction of CO_2 with H_2O at 333 K without H_2. The result shows that only 0.07 μmol g^{-1} of CH_4 and no CO product were formed after 8 h in condition.

By increasing the reaction temperature to 363 K, both CH_4 and CO are detected. Their product yields are 5.32 and 0.26 μmol g^{-1} for CH_4 and CO, respectively, after 8 h of reaction. It is accepted that photon irradiation is the primary source of energy in photocatalysis to generate the electron-hole pairs at an ambient temperature. However, the photocatalytic reactions proceed more efficiently at high temperatures because the surface reaction can be accelerated by raising the collision frequency and diffusion rate.[25] Furthermore, products do not easily be desorbed at low temperatures; on the contrary, it desorbs more readily at high temperatures. It should be mentioned that H_2O vapor plays a crucial role in the photocatalytic activity. Further raising the reaction temperature also increases the generated gaseous H_2O, resulting in the enhancement of photocatalytic activity. Several studies have focused on the reaction temperature dependence of

the photocatalytic activity.[25-27] Note that Anpo et al. also carried out the photoreduction of CO_2 with H_2O on various TiO_2 catalysts.[26] They reported that their enhancement of product yields corresponds to the reaction temperature and amount of gaseous H_2O, which is highly consistent with this study.

Investigation of photohydrogenation of CO_2 at 363 K in the presence of H_2 was also conducted. The result shows that it took 2 h for CO to reach a maximum yield (5.47 μmol g^{-1}), and then it gradually decreased. In general, CO is thermodynamically more favorable than CO_2.[11] Hence, it might be consumed by reacting with either H_2 or H_2O to produce CH_4, resulting in the observed decrease of CO yield. For the yield of CH_4, it is in a good linear relationship with the irradiation time. The CH_4 yield reaches to 28.72 μmol g^{-1} after 8 h in reaction. Such significant improvement of photocatalytic reaction is attributed to the presence of H_2, which is used immediately for the hydrogenation of CO_2. The reason is that hydrogenation of CO_2 is thermodynamically favorable and is a spontaneous reaction.

3.2 The amount Cu-loaded and its oxidation state on TiO_2 supports

The influence of amount CuO-loaded TiO_2 on photohydrogenation of CO_2 with H_2O was also examined at 363 K. As expected, Figure 9 shows that the catalysts with a CuO loading of 1 and 2 wt.% exhibited photocatalytic reactivity to produce CO and CH_4 with a yield of 4.0-5.0 and 19.3-14.6 μmol g^{-1}, respectively. Note that only 1.33 μmol g^{-1} of CO and 11.94 μmol g^{-1} of CH_4 were produced over TiO_2 under the same condition. It is well known that the recombination of the electron-hole pair will be reduced when Cu species is loaded on TiO_2. Hence, the photoactivity will be enhanced with the loading of Cu species. Additionally, Ti^{3+} species are an important

246 factor that influences the photocatalytic activity in the photohydrogenation of CO_2. The reason is
247 that the electron-rich Ti^{3+} species might transfer spontaneously an electron to surface adsorbed
248 CO_2 leading to an intermediate $CO_2^{\bullet-}$ species.[28] As it can be noticed, $CO_2^{\bullet-}$ species is supported
249 as the precursor of CO formation. It is important to emphasize that following the loading Cu
250 species on TiO_2 support, the ratio of Ti^{3+} species, which is shown in Figure 6(b), will increase
251 dramatically compared with TiO_2. Hence, the observed yield of CO was increased more than
252 threefold by Cu-loaded species. On the other hand, the surface hydroxyl content of photocatalyst
253 was observed to increase with the presence of Cu-loaded (Figure 6(c)). It is noted that the surface
254 hydroxyl is the crucial role to enhance the photocatalytic activity by generating the active
255 hydroxyl radicals.[29]

256 Although the adding CuO species improves significantly the activity, the addition of excess CuO
257 to TiO_2 was undesirable for the photoreaction. Firstly, one of the influential factors of this
258 dependence may be the CuO dispersion on TiO_2. The CuO dispersion usually decreases with
259 increasing loading amount because of the aggregation of some small CuO particles, resulting in
260 the reduced surface illumination of the photocatalyst. Note that BET surface area of
261 1%CuO/TiO_2 and 2%CuO/TiO_2 photocatalysts are 6.1 and 3.8 $m^2\ g^{-1}$, respectively (Table 1). A
262 loss of 38% of BET surface area was observed by increasing the loading CuO amount from 1%
263 to 2%. The previous study observed that $CuCl_2$ precursor, which was also used in this study, led
264 to being well-dispersed Cu at low loading only.[30, 31] At high loading, a significant amount of
265 CuO species aggregated on the surface of the support and obscured the pores of TiO_2. Secondly,
266 excess CuO might act as the recombination centers for electron-hole pairs, resulting in reduced
267 photoactivity.

The oxidation state of Cu species is also a key factor that determines their CO_2 photoreduction activity.[15] In this study, the pretreatment 1%CuO/TiO_2 by reducing CuO to Cu was found to be more efficient to generate CH_4 than that without pretreatment (Figure 10). The yield of CH_4 for Cu/TiO_2 was 28.72 μmol g^{-1}, which was enhanced 48.5% compared with that for CuO/TiO_2. To gain further insight into the transition of the nature of the copper species during the reaction, the photocatalysts was collected after the experiment for further XPS and UV-vis analysis. Figure 11 shows that the Cu2p peaks for spent CuO/TiO_2 photocatalyst, which was collected after the reaction, were shifted to lower binding energy than those for fresh CuO/TiO_2 photocatalyst. On the other hand, the Cu2p peaks for spent Cu/TiO_2 photocatalyst were shifted to higher binding energy than those for fresh Cu/TiO_2 photocatalyst. This result reveals that Cu^{1+} species could be generated during UV-light irradiation from a part of either Cu^0 or Cu^{2+} species.

$$\text{Photocatalyst} + h\nu \rightarrow h^+ + e^- \quad (3)$$

$$Cu^0 + h^+ \leftrightarrow Cu^{1+} + e^- \quad (4)$$

$$Cu^{2+} + e^- \leftrightarrow Cu^{1+} + h^+ \quad (5)$$

During the photoreaction, the holes and electrons from TiO_2 can be transferred to Cu^0 and Cu^{2+} species to keep a certain amount of their species oxidized and reduced, respectively, to Cu^{1+}.[32] The UV-vis analysis of above photocatalysts is also shown in Figure 11. In details, the UV-vis spectrum of the spent Cu/TiO_2 photocatalyst shows an increased intensity in the range of 410-590 nm, in compared with that of the fresh Cu/TiO_2 photocatalyst. This change indicates that a part of Cu^0 was oxidized to Cu^{1+} species.[19] Similarly, we also observed this phenomenon for spent CuO/TiO_2 photocatalyst, confirming the presence of Cu^{1+} species. The UV-vis result agrees with the XPS result. We final note that CuO-Cu_2O/TiO_2 and Cu-Cu_2O/TiO_2

photocatalysts system could be formed under UV-light irradiation (Figure 11). Briefly, the co-existence of different nature of Cu species has a significant influence on the photocatalytic activity by the enhanced separation and inhibited recombination of photogenerated electron-hole pairs. Moreover, it also exhibits outstanding the optical properties. Especially, the Cu-Cu_2O/TiO_2 structure is proposed can also further prolong the lifetime of electrons. The reason is that the electrons, which is generated by UV-light irradiation on the Cu_2O valence band, need to transfer to the media Cu first, and then further transfer to the valence band of TiO_2.[32] As a result, Cu-Cu_2O/TiO_2 had the highest photocatalytic performance, among candidate photocatalysts. Interestingly, Cu-Cu_2O/TiO_2 also performed an excellent selectivity to CH_4 yield. The reasons are that Cu^0 species could efficiently suppress the formation of CO,[33] while Cu^{1+} species is noted as an active site to promote the formation of CH_4 efficiently.[34]

3.3 Comparison of the photoreduction efficiency

The dependencies of products yield and PQE on different photocatalysts are shown in Figure 12. The results suggest that Cu-loaded TiO_2 reduces CO_2 more efficiently than TiO_2. The photohydrogenation activity is intensively related to the amount Cu-loaded and its oxidation state on TiO_2. The increased photocatalytic activity with the presence of Cu species can be explained as Cu species acting as electron traps responsible for accumulating the photo-generated electrons, and resulting in minimizing charge recombination electron-hole pairs. Additionally, the ratio of Ti^{3+} species in Cu-loaded TiO_2 was higher than that in TiO_2. This observation is attributed to the enhancement of CO formation. However, adding excess CuO/Cu to TiO_2 may face the low dispersion issue resulting in the activity inhibition. In the present, we observed that PQE achieved highest over 1%Cu/TiO_2 photocatalyst (0.13%).

Although the conditions for conducting experiments are different, it is worth comparing the photocatalytic activity regarding product rate in the literature (Table 2).[17, 35-41] We see that CO and CH_4 were formed as the main products. Despite substantial efforts have been devoted to improving the efficiency of this photocatalytic process, it is still lower than in natural photosynthesis. Hence, further research in this field is needed for enabling photohydrogenation / photoreduction of CO_2 in the future.

4. Conclusions

Cu species (Cu^0 and Cu^{2+}) were successfully loaded on the TiO_2 support and then evaluated for their potential to hydrogenation of CO_2. There might exist the interaction between the Cu species and TiO_2 support that enhancing a significant amount of Ti^{3+} rather than Ti^{4+} species in Cu-loaded TiO_2, in compared with TiO_2 photocatalysts. This property provides a chance to generate an intermediate $CO_2^{\bullet-}$ species, leading to the enhancement of CO_2 hydrogenation activity. Notably, CuO-Cu_2O/TiO_2 and Cu-Cu_2O/TiO_2 photocatalyst system, which was formed under UV-light irradiation, significantly enhanced photocatalytic activity by prolonging the lifetime of electrons. The co-existence of Cu^0 and Cu^{1+} species was beneficial to catalysis involving hydrogenation of CO_2 into desired renewable fuel (CH_4). Although the adding Cu species improves the activity significantly, the excess content of Cu to TiO_2 was undesirable for the photoreaction. To achieve the enhanced photocatalytic activity, the content of Cu species must be maintained at an appropriate low concentration (≤ 1wt.%), and the corresponding highest CH_4 yield was 28.72 μmol g^{-1}.

Acknowledgments

The authors kindly thank the Ministry of Science and Technology, Taiwan for financially supporting this research under the project MOST 103-2923-E-002-009-MY3 and the Grant Agency of the Czech Republic (14-35327J).

References

1. D. Lozano-Castelló, F. Suárez-García, Á. Linares-Solano and D. Cazorla-Amorós, in *Renewable Hydrogen Technologies*, ed. L. M. G. A. M. Diéguez, Elsevier, Amsterdam, 2013, DOI: http://dx.doi.org/10.1016/B978-0-444-56352-1.00012-X, pp. 269-291.
2. S. Kumar, in *Clean Hydrogen Production Methods*, Springer International Publishing, 2015, DOI: 10.1007/978-3-319-14087-2_1, ch. 1, pp. 1-9.
3. F. Amrouche, A. Benzaoui, P. Erickson, B. Mahmah, F. Herouadi and M. Belhamel, *Int. J. Hydrogen Energy*, 2011, **36**, 4094-4102.
4. A. Züttel, *Naturwissenschaften*, 2004, **91**, 157-172.
5. N. P. Gillett, V. K. Arora, D. Matthews and M. R. Allen, *J. Climate*, 2013, **26**, 6844-6858.
6. S. Protti, A. Albini and N. Serpone, *Phys. Chem. Chem. Phys.*, 2014, **16**, 19790-19827.
7. A. Züttel, P. Mauron, S. Kato, E. Callini, M. Holzer and J. Huang, *CHIMIA Int. J. Chem.*, 2015, **69**, 264-268.
8. S. Saeidi, N. A. S. Amin and M. R. Rahimpour, *J. CO2 Utilization*, 2014, **5**, 66-81.
9. T. Müller, W. Leitner, P. Markewitz and W. Kuckshinrichs, in *Carbon Capture, Storage and Use*, eds. W. Kuckshinrichs and J.-F. Hake, Springer International Publishing, 2015, DOI: 10.1007/978-3-319-11943-4_4, ch. 4, pp. 67-100.
10. X. Yang, S. Kattel, S. D. Senanayake, J. A. Boscoboinik, X. Nie, J. Graciani, J. A. Rodriguez, P. Liu, D. J. Stacchiola and J. G. Chen, *J. Am. Chem. Soc.*, 2015, **137**, 10104-10107.
11. Y.-H. Cheng, V.-H. Nguyen, H.-Y. Chan, J. C. S. Wu and W.-H. Wang, *Appl. Energy*, 2015, **147**, 318-324.

12. S.-H. Yu, C.-W. Chiu, Y.-T. Wu, C.-H. Liao, V.-H. Nguyen and J. C. S. Wu, *Appl. Catal. A: Gen.*, DOI: http://dx.doi.org/10.1016/j.apcata.2015.08.027.
13. K. Hirano, K. Inoue and T. Yatsu, *J. Photochem. Photobiol., A: Chem.*, 1992, **64**, 255-258.
14. J. C. S. Wu, H.-M. Lin and C.-L. Lai, *Appl. Catal. A: Gen.*, 2005, **296**, 194-200.
15. I. H. Tseng, J. C. S. Wu and H.-Y. Chou, *J. Catal.*, 2004, **221**, 432-440.
16. I. H. Tseng, W.-C. Chang and J. C. S. Wu, *Appl. Catal. B: Environ.*, 2002, **37**, 37-48.
17. F. Gonell, A. V. Puga, B. Julián-López, H. García and A. Corma, *Appl. Catal. B: Environ.*, 2016, **180**, 263-270.
18. S.-H. Wu and D.-H. Chen, *J. Colloid Interface Sci.*, 2004, **273**, 165-169.
19. H. Praliaud, S. Mikhailenko, Z. Chajar and M. Primet, *Appl. Catal. B: Environ.*, 1998, **16**, 359-374.
20. L. Chen, T. Horiuchi, T. Osaki and T. Mori, *Appl. Catal. B: Environ.*, 1999, **23**, 259-269.
21. B. Srinivas, B. Shubhamangala, K. Lalitha, P. Anil Kumar Reddy, V. Durga Kumari, M. Subrahmanyam and B. R. De, *Photochem. Photobiol.*, 2011, **87**, 995-1001.
22. V.-H. Nguyen, H.-Y. Chan and J. C. S. Wu, *J. Chem. Sci.*, 2013, **125**, 859-867.
23. M. You, T. G. Kim and Y.-M. Sung, *Cryst. Growth Des.*, 2010, **10**, 983-987.
24. H. Yamashita, M. Matsuoka, K. Tsuji, Y. Shioya, M. Anpo and M. Che, *J. Phys. Chem.*, 1996, **100**, 397-402.
25. V.-H. Nguyen, J. C. S. Wu and H. Bai, *Catal. Comm.*, 2013, **33**, 57-60.
26. M. Anpo, H. Yamashita, Y. Ichihashi and S. Ehara, *J. Electroanal. Chem.*, 1995, **396**, 21-26.
27. X. Fu, L. A. Clark, W. A. Zeltner and M. A. Anderson, *J. Photochem. Photobiol., A: Chem.*, 1996, **97**, 181-186.
28. Ş. Neaţu, J. A. Maciá-Agulló, P. Concepción and H. Garcia, *J. Am. Chem. Soc.*, 2014, **136**, 15969-15976.
29. W. Lu, S. Gao and J. Wang, *J. Phys. Chem. C*, 2008, **112**, 16792-16800.
30. X. Bokhimi, A. Morales, O. Novaro, T. López, O. Chimal, M. Asomoza and R. Gómez, *Chem. Mater.*, 1997, **9**, 2616-2620.
31. O. Ola and M. Mercedes Maroto-Valer, *Catal. Sci. Technol.*, 2014, **4**, 1631-1637.

32. Z. Xi, C. Li, L. Zhang, M. Xing and J. Zhang, *Int. J. Hydrogen Energy*, 2014, **39**, 6345-6353.
33. G. Wu, T. Chen, G. Zhou, X. Zong and C. Li, *Sci. China, Ser. B: Chem.*, 2008, **51**, 97-100.
34. S. Zhu, S. Liang, Y. Tong, X. An, J. Long, X. Fu and X. Wang, *Phys. Chem. Chem. Phys.*, 2015, **17**, 9761-9770.
35. D. Liu, Y. Fernández, O. Ola, S. Mackintosh, M. Maroto-Valer, C. M. A. Parlett, A. F. Lee and J. C. S. Wu, *Catal. Comm.*, 2012, **25**, 78-82.
36. F. Bi, M. F. Ehsan, W. Liu and T. He, *Chin. J. Chem.*, 2015, **33**, 112-118.
37. K. Teramura, S.-i. Okuoka, H. Tsuneoka, T. Shishido and T. Tanaka, *Appl. Catal. B: Environ.*, 2010, **96**, 565-568.
38. Q. Liu, Y. Zhou, Z. Tian, X. Chen, J. Gao and Z. Zou, *J. Mater. Chem.*, 2012, **22**, 2033-2038.
39. C. Zhang, Q. Zhang, S. Kang, B. Li, X. Li and Y. Wang, *ECS Solid State Lett.*, 2013, **2**, M49-M52.
40. S. K. Parayil, A. Razzaq, S.-M. Park, H. R. Kim, C. A. Grimes and S.-I. In, *Appl. Catal. A: Gen.*, 2015, **498**, 205-213.
41. T. Wang, X. Meng, G. Liu, K. Chang, P. Li, Q. Kang, L. Liu, M. Li, S. Ouyang and J. Ye, *J. Mater. Chem. A*, 2015, **3**, 9491-9501.

412 **Tables and Figures**

413 **Table 1.** The properties of TiO_2 supports

Entry	Photocatalysts	BET ($m^2 g^{-1}$)	TiO_2 crystalline size (nm)
1	TiO_2	5.2	31.4
2	1%CuO/TiO_2	6.1	32.6
3	2%CuO/TiO_2	3.8	32.6
4	1%Cu/TiO_2	6.3	34.0
5	2%Cu/TiO_2	5.1	33.9

414

415 **Table 2.** The performance comparison of photocatalytic activity

Entry	Catalysts	Conditions			Products (μmol g^{-1} h^{-1})	PQE (%)	Ref. / Year
		Reaction medium	Light source	Temp. (K)			
1	Cu/TiO_2	H_2O (5 mL), H_2 (0.01 atm), saturated CO_2 (1 atm)	11SC-1 pen-ray lamp: 254 nm; 12 mW cm^{-2}	363	**CO**: 0.54 **CH_4**: 3.59	0.13	This study
2		H_2O (5 mL), saturated CO_2 (1 atm)			**CO**: 0.03 **CH_4**: 0.67	0.03	
3	Cu/TiO_2	H_2O (200 mL), saturated CO_2 (1 atm)	8 W UVA: 3.25 mW cm^{-2}	–	**CH_4**: 0.03	–	[35] / 2012
4	Cu_2O/TiO_2	H_2O (100 mL), saturated CO_2 (1.25 atm)	300 W xenon lamp (PLS-SXE300, $\lambda \geq$ 420 nm)	288	**CH_4**: 0.16		[36] / 2015
5	$3.0Cu\text{-}TiO_2$	H_2O (25 mL) under a CO_2 atmosphere (1.4 bars)	Hg lamp (125 W)	298	**CO**: 0.3 **CH_4**: 0.3 **H_2**: 0.3	–	[17] / 2016
6	$LiTaO_3$	CO_2 (150 μmol), H_2 (50 μmol)	200 W Hg-Xe lamp (UVF-204S Type C)	303	**CO**: 0.42	–	[37] / 2010
7	RuO_2 –Pt/ $Zn_{1.7}GeN_{1.8}O$	H_2O (0.4 ml), saturated CO_2 (1 atm)	300 W Xe arc lamp ($\lambda > 420$ nm)	–	**CH_4**: 4.58	0.03	[38] / 2012
8	TiO_2-GCM	H_2O (5 ml), saturated CO_2 (1 atm)	300 W Xe arc lamp	303	**CH_4**: 2.06	–	[39] / 2013
9	C,N-TNT06	CO_2 and H_2O vapors (80% humidity)	100 W Xenon with an AM 1.5 filter	–	**CH_4**: 9.75	–	[40] / 2015
10	Co-doped TiO_2	H_2O (3 ml), a pure CO_2 gas (80 kPa)	300 W xenon arc lamp with an L-42 glass filter	–	**CO**: 0.34 **CH_4**: 0.18	–	[41] / 2015

Abbreviation: PQE: Photoreduction quantum efficiency, –: lack of information.

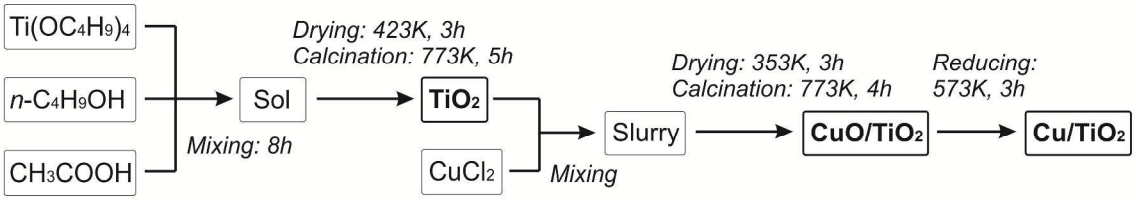

Scheme 1. The flow chart for synthesis procedure of photocatalysts.

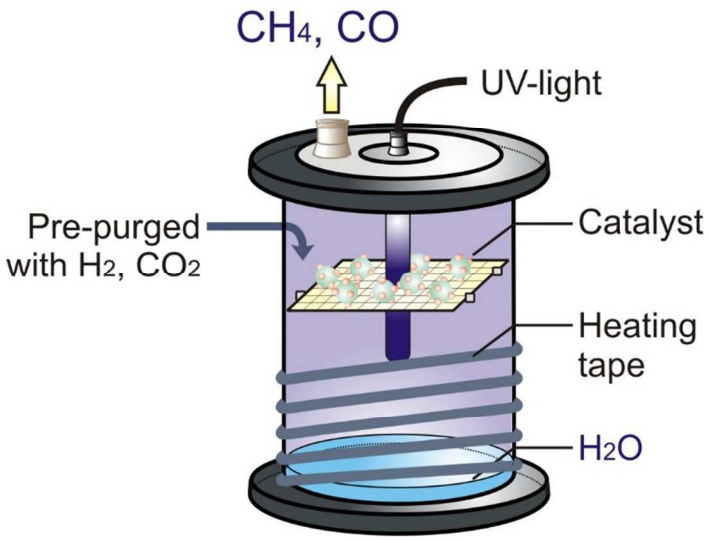

Figure 1. The diagram of a single Pyrex photoreactor system.

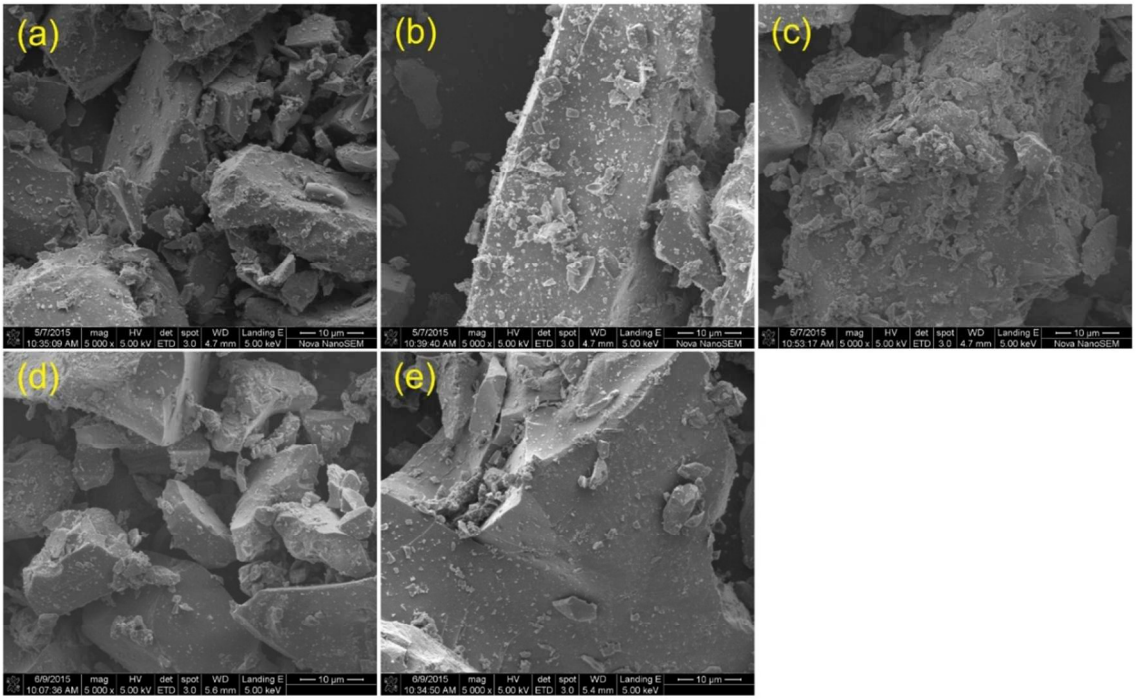

421

422 **Figure 2**. SEM images of (a) TiO_2, (b) 1%CuO/TiO_2, (c) 2%CuO/TiO_2, (d) 1%Cu/TiO_2, and (e)
423 2%Cu/TiO_2 photocatalysts.

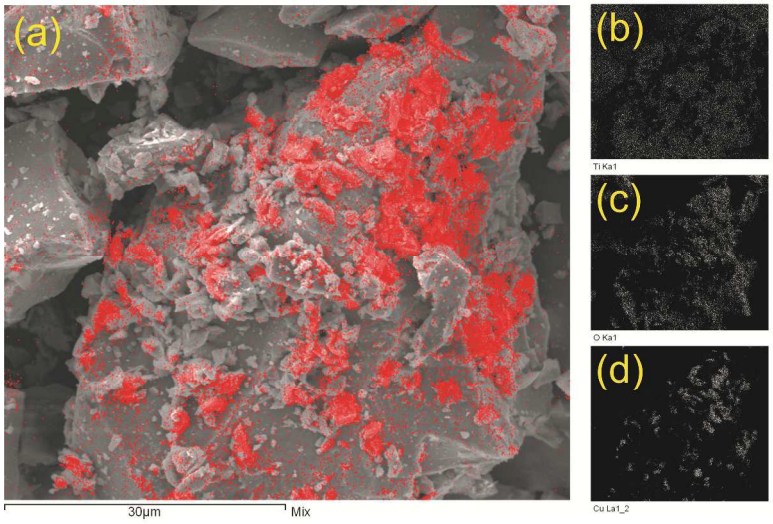

424

425 **Figure 3**. SEM mapping photograph for 2%CuO/TiO_2 photocatalyst: (a) SEM image of
426 2%CuO/TiO_2 with Cu mapping, and elemental mapping images of (b) Ti, (c) O, and (d) Cu.

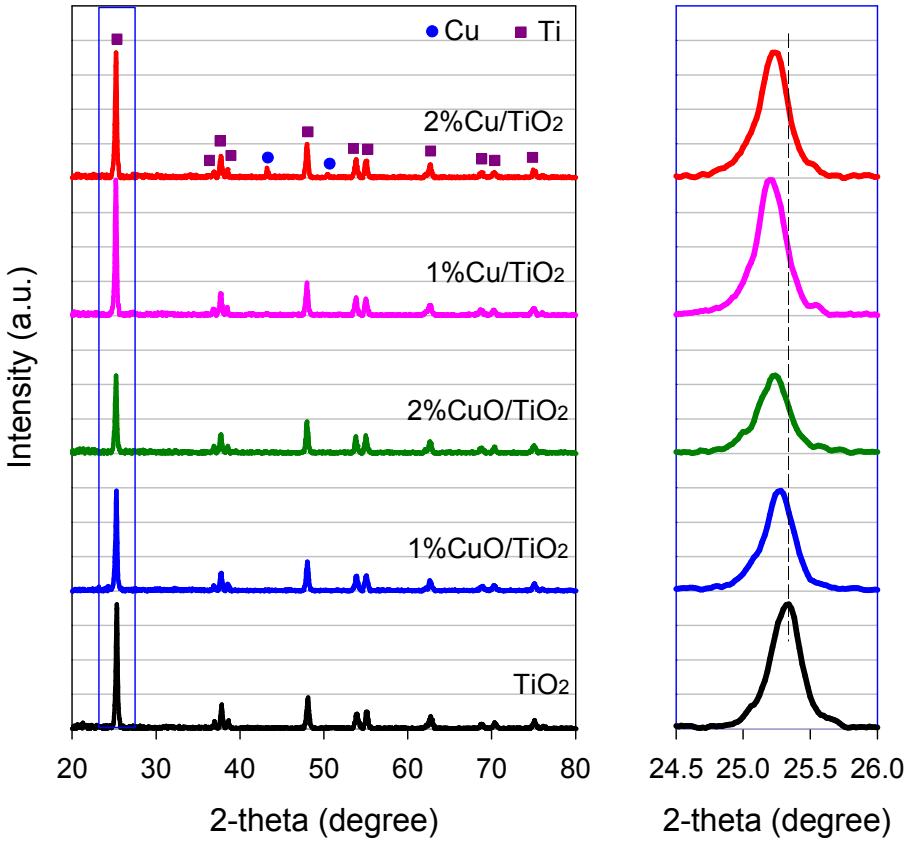

Figure 4. XRD patterns of TiO_2, 1%CuO/TiO_2, (c) 2%CuO/TiO_2, 1%Cu/TiO_2, and 2%Cu/TiO_2 photocatalysts. The inset depicts the shift of the (101) planes of TiO_2 supports.

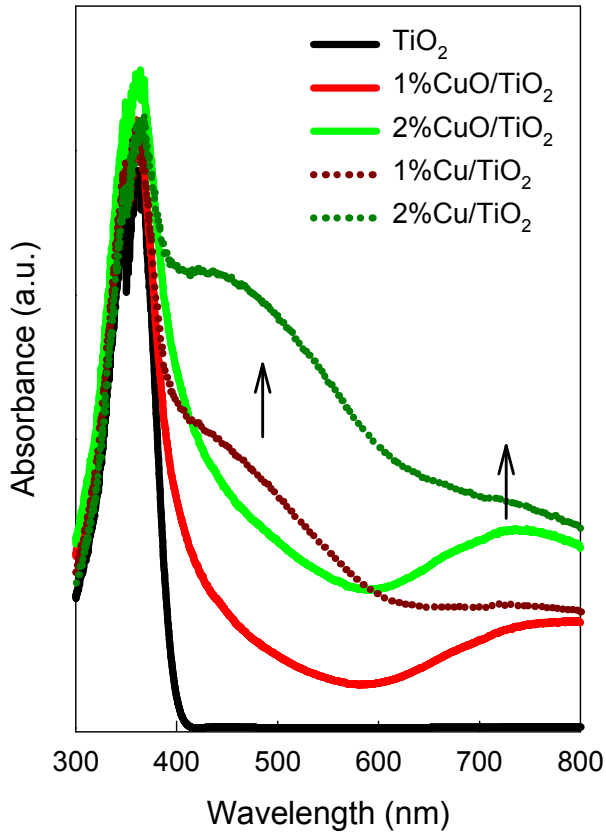

430

431 **Figure 5**. UV-vis spectra of TiO_2, 1%CuO/TiO_2, (c) 2%CuO/TiO_2, 1%Cu/TiO_2, and 2%Cu/TiO_2

432 photocatalysts.

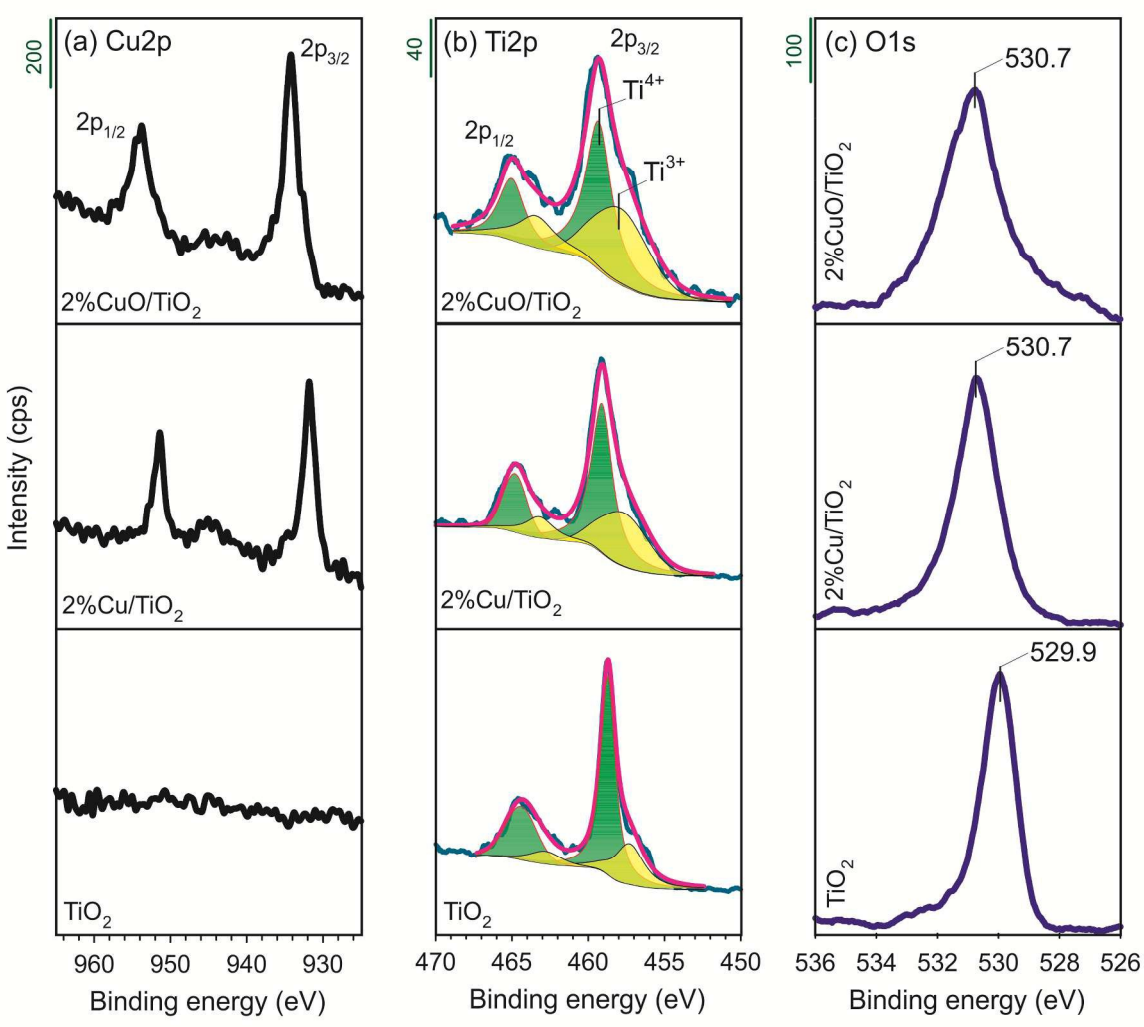

433

434 **Figure 6**. XPS spectra of (a) Cu2p, (b) Ti2p and (c) O1s for TiO_2, 2%Cu/TiO_2, and

435 2%CuO/TiO_2 photocatalysts.

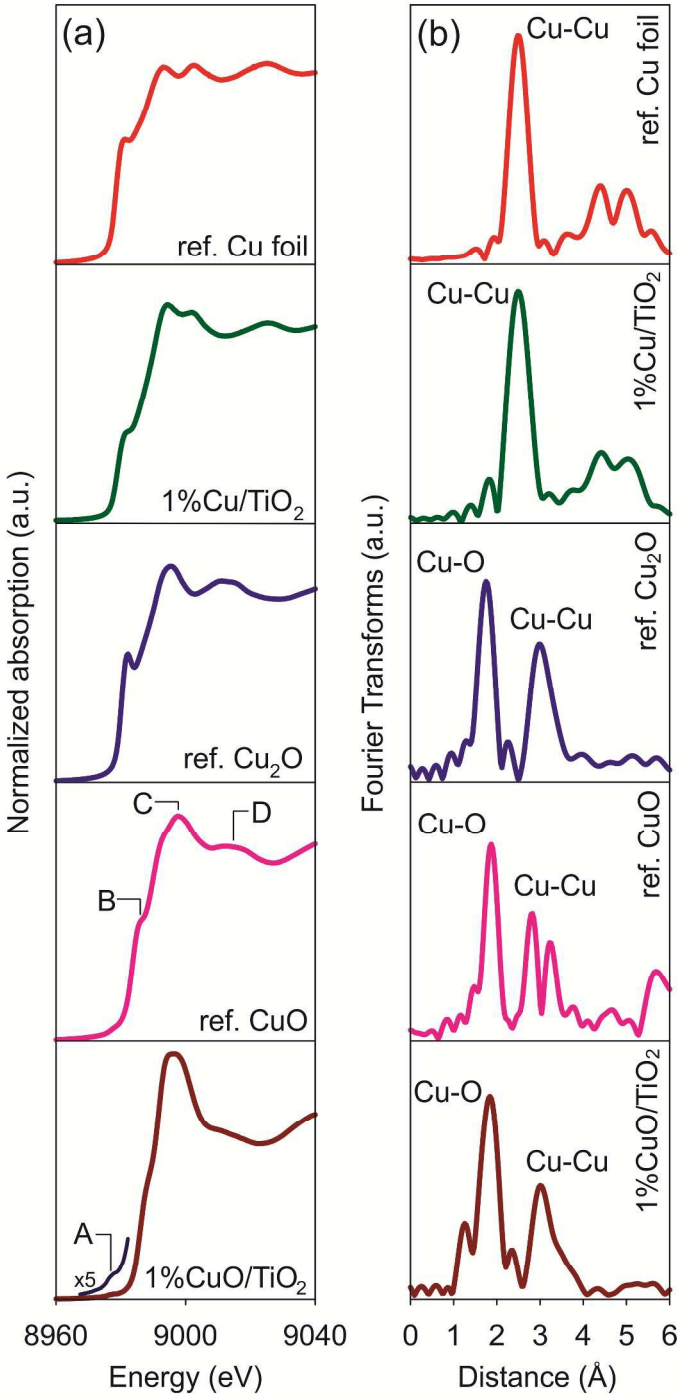

Figure 7. (a) Normalized Cu K-edge XANES spectra and (b) Fourier transforms of Cu K-edge EXAFS spectra for 1%Cu/TiO_2 and 1%CuO/TiO_2 photocatalysts, together with Cu metal foil, Cu_2O, and CuO references.

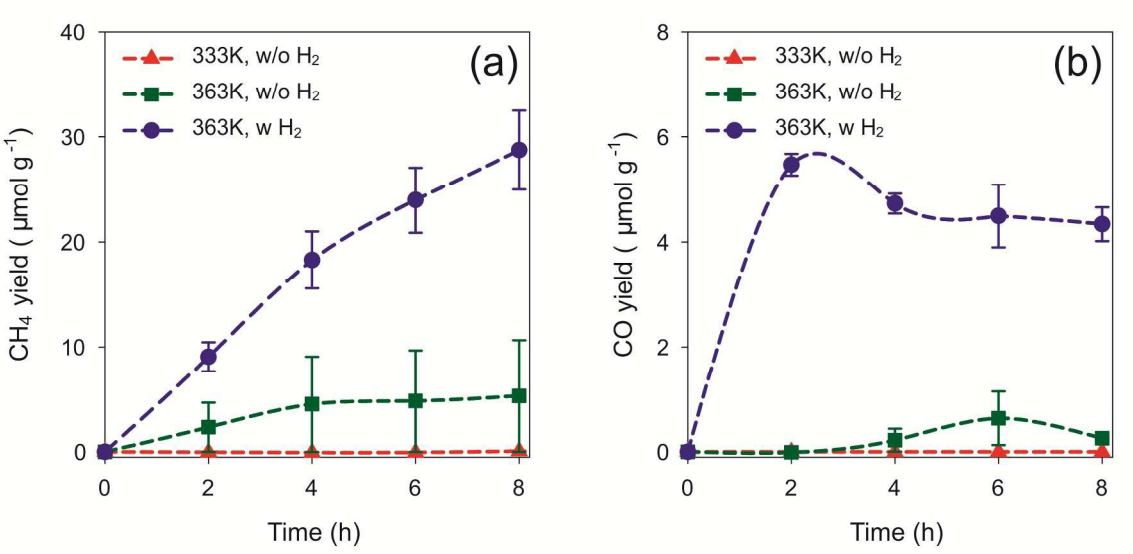

Figure 8. Reaction time profiles of the photocatalytic reduction of CO_2 with H_2O in the presence/absence of H_2 under different temperature to produce (a) CH_4 and (b) CO on 1%Cu/TiO_2 photocatalyst.

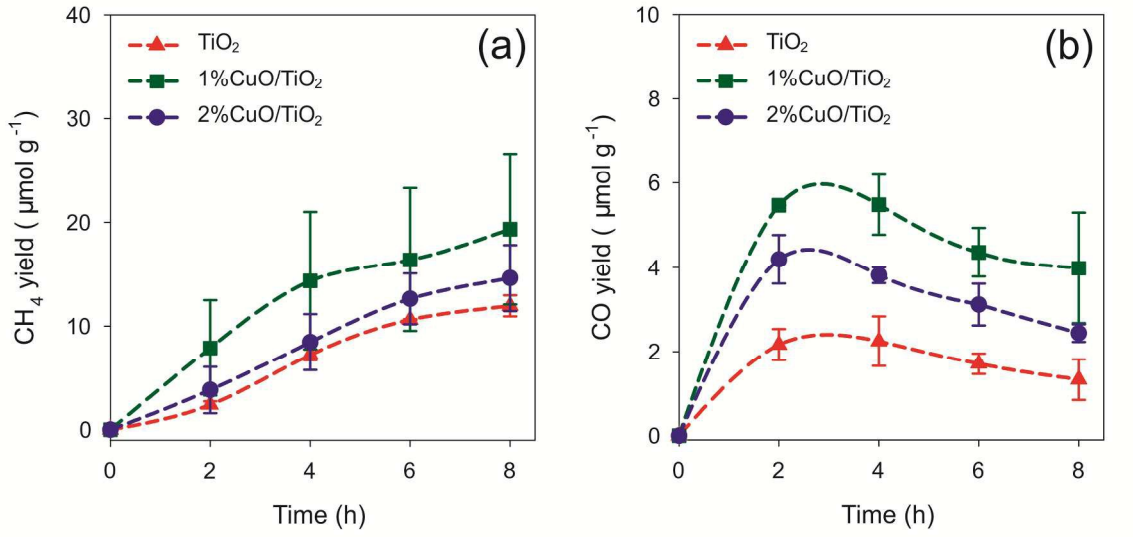

Figure 9. Reaction time profiles of the photocatalytic reduction of CO_2 with H_2O and H_2 to produce (a) CH_4 and (b) CO on different amount of CuO loaded TiO_2 photocatalysts.

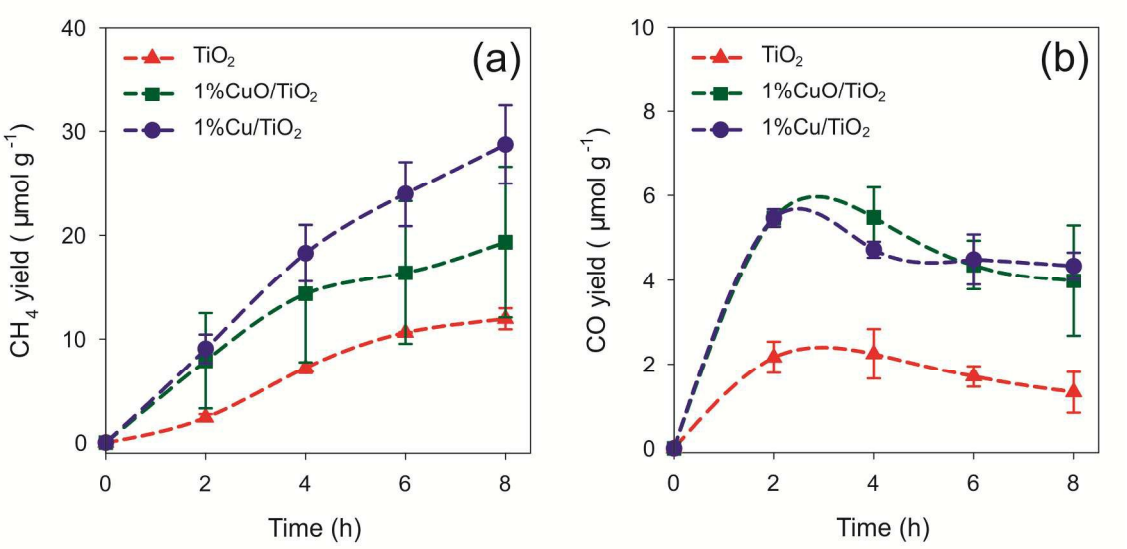

447

448 **Figure 10**. Reaction time profiles of the photocatalytic reduction of CO_2 with H_2O and H_2 to
449 produce (a) CH_4 and (b) CO on different Cu oxidation state photocatalysts.

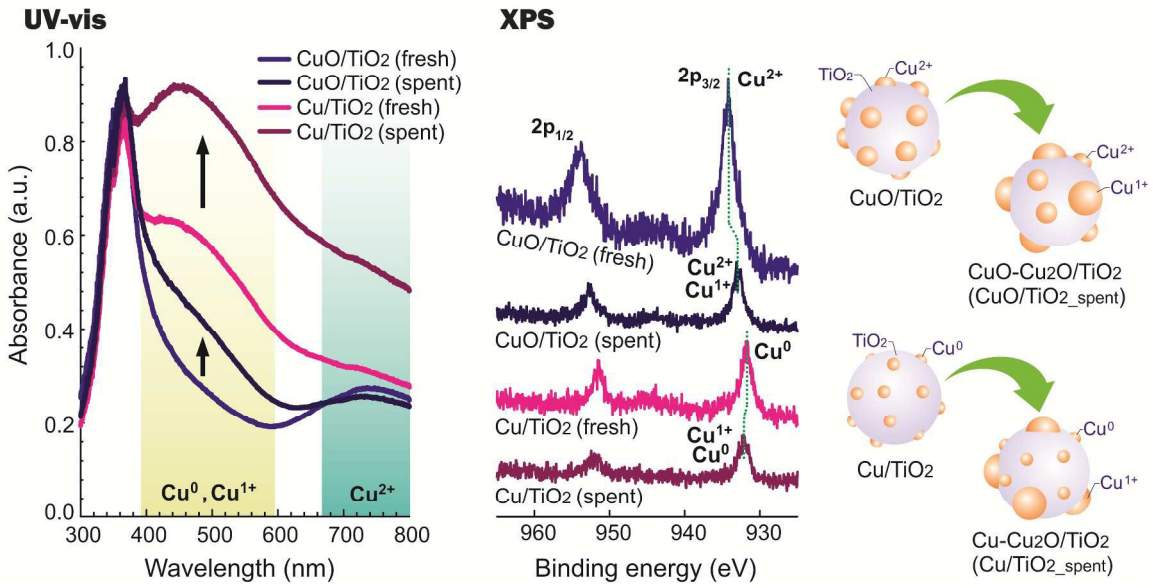

450

451 **Figure 11**. The transition of the nature of Cu species during the photoreaction.

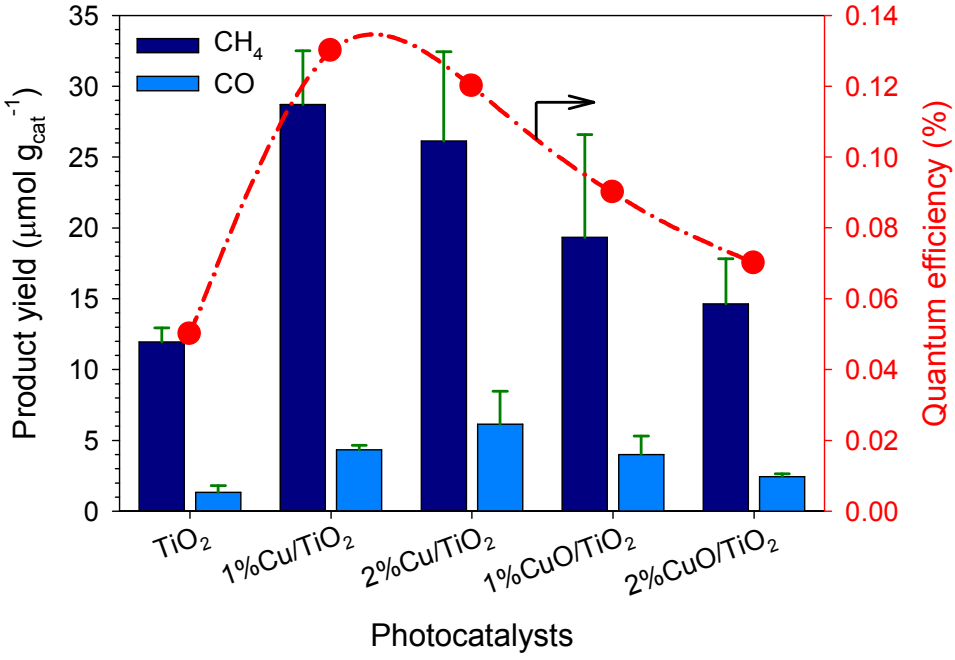

452

453 **Figure 12**. Performance comparison of the products yields (after 8 h in reaction) and the
454 quantum efficiency on different photocatalysts.